Available online at www.sciencedirect.com

ScienceDirect

Advances in Space Research 72 (2023) 5030–5046

ADVANCES IN SPACE RESEARCH (a COSPAR publication)

www.elsevier.com/locate/asr

Precise orbit determination of Spire nano satellites

Daniel Arnold [a,*], Heike Peter [b], Xinyuan Mao [a,1], Alexandra Miller [a], Adrian Jäggi [a]

[a] Astronomical Institute, University of Bern, Sidlerstrasse 5, Bern CH-3012, Switzerland
[b] PosiTim UG, In den Löser 15, Seeheim-Jugenheim 64342, Germany

Received 15 June 2023; received in revised form 7 September 2023; accepted 8 October 2023
Available online 11 October 2023

Abstract

Spire Global, Inc. operates a growing fleet of currently more than 100 CubeSats in different low Earth orbits for commercial Earth observation. These satellites are equipped with dual-frequency GPS receivers and an attitude determination and control system, allowing for precise orbit determination. For three different satellites and a time span of six months we analyze the performance and quality of the on-board collected GPS and attitude data and employ it for precise orbit determination using the Bernese GNSS Software and Napeos, two independent state-of-the-art GNSS processing software packages. We describe technical details crucial for POD and present and compare the in-flight calibrated phase center variation maps. Reduced-dynamic and kinematic orbits are then inter-compared between the two software packages as well as to the orbit solutions produced by Spire Global. We report pseudo-range and carrier phase residuals at the level of 3–4 m and 8–9 mm RMS and a good agreement between the reduced-dynamic and kinematic orbits of around 5 cm 3D RMS. The reduced-dynamic orbit positions and velocities produced with the two employed software packages agree in average on the level of 6–7 cm and 0.05–0.07 mm/s 3D RMS, while the comparison to the orbits produced by Spire Global is markedly worse with 27–30 cm and 0.32–0.36 mm/s 3D RMS. The presented results are an encouraging first step towards using GPS data from the Spire constellation for geodetic, geophysical and ionospheric applications.
© 2023 COSPAR. Published by Elsevier B.V. This is an open access article under the CC BY license (http://creativecommons.org/licenses/by/4.0/).

Keywords: Low Earth orbiting satellites; Spire; CubeSats; Precise orbit determination; GNSS

1. Introduction

The use of small satellites, i.e., artificial satellites with weights less than 500 kg, has witnessed a remarkable growth over the past few years (Kopacz et al., 2020). Nano satellites, small satellites with very low weight between 1 and 10 kg, are nowadays considered for numerous purposes. Due to advances in micro-electronics, these comparably inexpensive satellites become more and more powerful and find gradually new applications, such as in communication and data networks (Akyildiz and Kak, 2019; Saeed et al., 2020), or various kinds of Earth observations (see, e.g., Pastena et al. (2020), Wu et al. (2021), Azami et al. (2022), Palfreyman et al. (2022)). The low price also enables to run small satellites in megaconstellations, with a potential to significantly increase global coverage and timeliness.

The concept of CubeSats, a class of nano satellites which are built from standardized basic units (U) of 10 cm × 10 cm × 10 cm cubes with weights typically less than 1.33 kg (Johnstone, 2022), was introduced by California Polytechnic State University and Stanford University. By relying on simple and standardized parts, CubeSats helped to lower costs of nano satellites and to decrease their development time.

E-mail address: daniel.arnold@unibe.ch (D. Arnold).
[1] Now at: Technology and Engineering Center for Space Utilization, Chinese Academy of Sciences, Dengzhuang South Road 9, Beijing 100094, China.

https://doi.org/10.1016/j.asr.2023.10.012
0273-1177/© 2023 COSPAR. Published by Elsevier B.V.
This is an open access article under the CC BY license (http://creativecommons.org/licenses/by/4.0/).

The majority of nano satellites is launched into Low Earth Orbits (LEOs, Kulu, 2022). Nowadays, many of these satellites carry dual-frequency GNSS (Global Navigation Satellite System) receivers of increasingly good quality. This, together with attitude determination systems, allows for precise orbit determination (POD) applications with meanwhile impressive accuracies. A natural question to ask then in the presence of such growing megaconstellations of small satellites is, whether the data collected by the on-board sensors can be exploited for scientific applications different to what the satellites were designed for. As an example, Kłopotek et al. (2021) have studied the use of LEO CubeSats from the currently built up Astrocast constellation (designed to establish a global satellite network for Internet of things applications) for co-locations in space in order to improve the estimation of global geodetic parameters.

In that context, ESA invoked in 2021 an Announcement of Opportunity (AO) for Spire data, upon which the Astronomical Institute of the University of Bern (AIUB) was granted access to Spire data in the frame of the proposed project "Precise Orbit Determination of the Spire Satellite Constellation for Geodetic, Geophysical, and Ionospheric Applications" (ID No. 66978).

Spire Global, Inc., a public company with headquarters in San Franscisco, U.S., operates a growing fleet of currently more than 100 CubeSats intended for AIS (Automatic Identification System)-based tracking of sea vessels, ADS-B (Automatic Dependent Surveillance)-based surveillance of aircraft, as well as for performing GNSS-based radio occultation (RO) measurements (Cappaert, 2020). The Spire nano satellites build upon the in–house developed Low Earth Multi-Use Receiver (LEMUR) 3U CubeSat platform (Angling et al., 2021) and have a designed satellite lifetime of 3–5 years. The satellites are orbiting the Earth in LEO altitudes between 400 km and 650 km.

The Spire CubeSats carry an in–house developed dual-frequency GPS receiver. This receiver is attached to a zenith GNSS antenna for POD and to side-mounted GNSS antennas for RO measurements, see Fig. 1. The fact that this large and growing number of satellites is equipped with dual-frequency GNSS receivers offers the potential for interesting applications. E.g., Forsythe et al. (2020) investigated on the determination of ionospheric electron densities from Spire RO observations, showing good agreement with independent ground-based measurements. Another treatise of Spire RO-based methods to characterize the ionosphere can be found in Angling et al. (2021). The authors employ Spire RO measurements for total electron content recovery, as well as characterization of the ionosphere E region and ionospheric scintillations. The potential to use Spire data for the determination of thermospheric densities and the assimilation of these into neutral density models is explored in Sutton et al. (2021). Allahvirdi-Zadeh et al. (2022) provide a detailed analysis of the stability of Spire CubeSat receiver clock estimates – with RO applications in mind – and propose methods to improve the stabilities. They show that vertical atmospheric profiles in the upper troposphere-lower stratosphere are comparable to profiles obtained with COSMIC-2 (Schreiner et al., 2020).

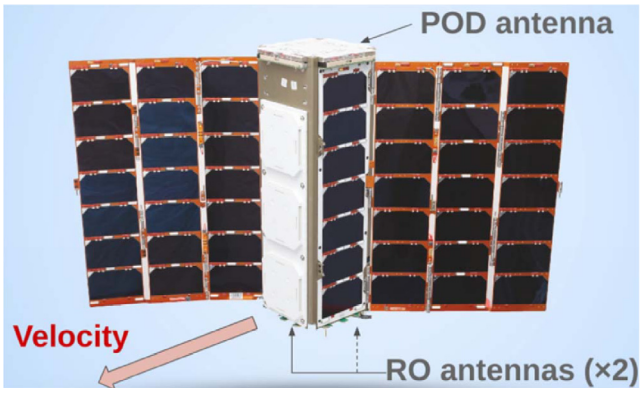

Fig. 1. The STRATOS antenna locations on a Spire LEMUR2v3.4 satellite. From Angling et al. (2021).

The present study focuses on the GPS-based POD of CubeSats from the Spire constellation. The data provided by Spire in the frame of the ESA AO comprise 9 satellites at three different altitudes, 8 of them in Sun-synchronous orbits at two different local times of ascending node (LTAN), as well as one satellite at an inclined orbit. GPS and attitude data of three exemplary satellites, flight model (FM)099, FM103 and FM115, for the 6 months period of May-October 2020 were processed to obtain precise orbit ephemerides. The three selected satellites are representative for the three orbital altitudes, the two LTANs and the two inclinations (see also Table 1). The processing was done using two independent state-of-the-art software packages, Bernese GNSS Software (BSW, Dach et al., 2015) and ESA's Napeos software (Springer et al., 2011), which allowed for an intercomparison of the resulting orbit solutions. If no external validation, e.g., with Satellite Laser Ranging, is possible, such an intercomparison of independently derived orbit solutions is a way to assess orbit quality, even if it is only in terms of consistency rather than absolute accuracy. The orbits were also compared to the official Level 1B satellite ephemerides produced and provided by Spire (leoOrb product). The purpose of the study is to characterize the quality of the GPS and attitude data of the Spire CubeSats and thereof derived precise trajectories. It aims to collect specific information crucial for Spire satellite POD and to complement the foundation for further scientific applications of the Spire GPS and attitude data and trajectories. Of particular interest can be time-variable Earth gravity field determination, for which POD is always a core part. The large number of satellites enables a good spatial (and temporal) coverage of the Earth and the diversity of orbit inclinations is interesting in the prospect of decorrelating highly correlated gravity field parameters (Gunter et al., 2011). Today, monthly high-quality Earth gravity field solutions since 2002 can

Table 1
The three Spire satellites analyzed in this study. FM099 and FM103 are in Sun-synchronous orbits with LTAN 09:30 and 15:05, respectively.

Spire FM	NORAD ID	S/C name	COSPAR ID	Orbit insertion date	Altitude	Inclination
099	44084	LEMUR-2-JOHANLORAN	2019-018G	2019-04–01	484.8 × 501.6 km	97.4°
103	44402	LEMUR-2-WANLI	2019-038S	2019–07-05	513.3 × 546.5 km	97.6°
115	44855	LEMUR-2-JPGSQUARED	2019-089D	2019–12-11	570.5 × 578.0 km	37.0°

be derived from the dedicated missions Gravity Recovery And Climate Experiment (GRACE, Tapley et al., 2004) and its successor mission GRACE-Follow On (GRACE-FO, Landerer et al., 2020). However, next to shorter gaps in the GRACE and GRACE-FO time series, there exists a gap of about one year between GRACE and GRACE-FO, and GRACE-FO has two single points of failures (GRACE-FO D Integrated Processing Unit and GRACE-FO C accelerometer), which could end the mission at any time. Gravity recovery from non-dedicated LEO missions, e.g., like the ESA mission Swarm (da Encarnação et al., 2020; Grombein et al., 2022), is thus an important means to fill existing gaps and to guarantee continuous Earth gravity field observations. Naturally, the question arises how beneficial the addition of (part of) the Spire constellation could be to improve gravity recovery from non-dedicated missions.

Another interesting scientific application of Spire data to be explored is the improved derivation of terrestrial reference frames (TRF) in fully combined global analyses of terrestrial GNSS data together with LEO GNSS data. Today, LEO satellites are not used at all for TRF computations, but it has been shown by several groups that the addition of the LEO layer – and in particular with various orbital inclinations – is beneficial when recovering parameters of geodetic or geophysical interest, such as geocenter coordinates (Hugentobler et al., 2005; Kuang et al., 2015; Haines et al., 2015; Männel and Rothacher, 2017; Huang, 2022). An in-depth understanding of all POD-relevant details is a prerequisite to fully exploit the potential of the Spire constellation for such purposes.

Finally, another scientific application of Spire data (also addressed in the frame of the formerly mentioned ESA AO proposal), is the determination of topside ionospheric electron densities on a global scale using LEO data (Schreiter et al., 2023). Here, the Spire constellation is interesting, because it has the potential to significantly improve the coverage in local time and because the low-elevation GPS data allows to better probe the lower altitude regimes of the ionosphere (notice that the Spire receivers track a significant amount of GPS observations below the local horizon of the antenna, see Section 2.4). A thorough understanding and characterization of the GPS data tracked by the Spire satellites is prerequisite for such ionosphere modelling attempts.

This paper is structured as follows. In Section 2 the satellite and instrument properties relevant for POD are presented, and the GPS and attitude data quality and completeness are studied. Section 3 gives details about the general POD methods employed and Section 4 presents results for the in-flight calibrations of GPS POD antennas. Section 5 summarizes the important POD results, including a discussion of observation residuals and internal orbit consistency, as well as comparisons between the BSW- and Napeos-derived orbits, and the orbits provided by Spire. Also an analysis of empirical and non-gravitational accelerations, as well as receiver clock properties and stabilities is presented. Section 6 discusses the impact of the numerous gaps present in the Spire data on the determined orbit, and Section 7 draws the summary and conclusions.

2. Satellite properties

This section gives an overview on the satellite body and instrument properties relevant for POD, and presents analyses of the GPS and attitude data completeness and tracking performance.

2.1. Satellite body

In the frame of this study the POD-related data of three Spire satellites, FM099, FM103 and FM115, were analyzed. Table 1 shows some general information about these satellites. These are all second-generation (LEMUR2) 3U CubeSats with satellite body dimensions of $10 \times 10 \times 34$ cm (Angling et al., 2021). The considered satellites all have the satellite bus major version 3.4, which was used from FM091 onwards (see Fig. 1). In the spacecraft body-fixed reference frame (SBF)[2] the center of mass (CoM) location for the major version 3.4 bus reads $\mathrm{CoM}_x = +2.14$ mm, $\mathrm{CoM}_y = -1.02$ mm, $\mathrm{CoM}_z = -22.21$ mm, and the total mass amounts to 5149 g (V. Nguyen, personal communication, October 2021).

2.2. GNSS instrument and data

The Spire nano satellites are equipped with a STRATOS dual-frequency GNSS receiver, which is designed and developed by Spire (Angling et al., 2021). The receiver is capable to track signals from the GPS, GLONASS, Galileo and QZSS systems, but currently for POD only GPS satel-

[2] The SBF is a right-handed orthogonal frame with origin at the geometric center of the satellite bus, with the x_{SBF}-axis normal to the surface containing the front RO antenna (nominal velocity direction) and the z_{SBF}-axis normal to the surface opposite to the POD antenna (nadir-pointing). y_{SBF} completes the right-handed orthogonal frame.

lites are tracked. The receiver is connected to three antennas. The zenith-looking POD antenna is a single patch, right hand circularly polarized (RHCP) antenna. In addition, two RO antennas are mounted in forward and backward velocity direction, each consisting of three RHCP patches, see Fig. 1. In this study, only tracking data from the zenith-looking POD antenna will be analyzed. The GNSS data is provided in Receiver Independent Exchange Format (RINEX, Romero, 2020) 3.02 files created by Spire. They contain the GPS pseudorange and carrier phase observations on L1 C/A and L2 L2C(L) (RINEX-3 observation codes C1C, L1C, C2L and L2L, respectively) at a data rate of 1 Hz.

The POD antenna of all considered Spire satellites is of version LEMUR3.1.0. In the SBF the location of the frequency-specific antenna reference point (ARP) reads $\mathrm{ARP}_x = -2.64$ mm, $\mathrm{ARP}_y = +3.50$ mm, $\mathrm{ARP}_z = -185.37$ mm for L1 and $\mathrm{ARP}_x = -1.45$ mm, $\mathrm{ARP}_y = +5.76$ mm, $\mathrm{ARP}_z = -175.58$ mm for L2 (V. Nguyen, personal communication, October 2021). For the POD, the GPS ARP was selected to be the phase center location on L1, and the difference vector from the L1 to the L2 phase center location was considered in the L2 phase center offset (PCO). In the antenna reference frame (ARF)[3] the L1 and L2 PCO values thus read $\mathrm{PCO}_{\mathrm{L1}} = (0, 0, 0)$ mm and $\mathrm{PCO}_{\mathrm{L2}} = (1.19, -2.26, -9.79)$ mm.

2.3. Attitude data

Each Spire LEMUR2 satellite is equipped with an attitude determination and control system (ADCS), which is used to estimate the satellite attitude based on sun sensors, magnetometers and Earth-horizon sensors. To control the attitude, reaction wheels and magnetotorquers are employed (Angling et al., 2021). The measured attitude is provided in quaternion information at 1 Hz sampling. A peculiarity of the attitude data is that the provided quaternions do not, as common practice, describe the rotation between the SBF and an inertial reference frame (e.g., J2000), but between the SBF and the Local Vertical-Local Horizontal (LVLH) reference frame. The latter has its origin at the satellite CoM, the z-axis pointing antiparallel to the geocentric satellite position vector (positive towards center of the Earth), the x-axis in the orbital plane, perpendicular to the z-axis and in velocity direction, and the y-axis complementing the right-handed orthogonal system. Since the LVLH reference frame is always related to a specific satellite trajectory, the positions and velocities of this specific trajectory are in principle required to deduce the rotation into an inertial frame (required for POD). Spire used for that purpose an SGP4 (Simplified General Perturbations model, Hoots and Roehrich, 1980) propagation of Two Line Elements (TLEs) (V. Nguyen, personal communication, October 2022). For the POD performed in this study, the a priori orbit solutions (computed as part of the POD process) were used for the LVLH frame realizations instead. To quantify the introduced error due to the slightly inconsistent LVLH frame realizations, a TLE-based orbit for FM099 on May 1, 2020 was used to compute the rotation matrices relating the satellite-fixed and the inertial reference frame. This orbit differs by up to about 1500 m from the precise orbit computed in this study. Comparing the TLE- and precise orbit-derived rotations, the Euler angles differ by less than 0.7°. Given an offset of the POD GPS antenna from the center of mass of roughly 15 cm, the corresponding roll and pitch errors introduce an error in the inertial position of the GPS antenna of less than 2 mm, which is neglected here.

The attitude of the Spire satellite is characterized by regular once-per-orbit yaw flips, i.e., rotations of the satellite by about 180° around the SBF z-axis. Typically, the times during which the satellites are flying "forward" (i.e., pointing the SBF x-axis in velocity direction) and "backward" are roughly similar, but in particular FM099 and FM103 spend generally more time flying "backward" during an orbit. While these yaw flips do not induce large changes of the inertial location of the GPS antenna, they are important to take into account when estimating or using antenna phase center variations (see Section 4), or when using the attitude information for the modeling of non-gravitational forces. The roll and pitch angles, i.e., the rotation angles around the SBF x- and y-axes, are typically within a few degrees only.

2.4. Data availability and tracking performance

The processing of GPS and attitude data for POD was performed in daily batches. GPS data is provided by Spire in RINEX files spanning data arcs of lengths between less than 1 min and about 2 h (Level 1A podObs product, version 6.01). Due to the grouping of raw data performed by Spire (Spire, 2021), different such RINEX files usually contain overlapping data points. Table 2 gives on overview on the available GPS data for the three considered Spire satellites and the analyzed time span. While for FM103 GPS data is available on each of the 184 analyzed days, the data of FM099 and FM115 are missing for 23 and 84 days, respectively. Table 2 also shows the average amount of epochs for which GPS data are available per 24 h, counting all epochs, as well as only epochs with at least 1 or 4 GPS satellites tracked on both L1 and L2. Furthermore, it can be seen that for 0.4–0.6 % of epochs only measurements on GPS L1 are available. In average, the duty cycles (percentages of available epochs) for the three satellites amount to about 69–75 %. Thus, the analyzed Spire GPS data are affected by significant gaps. These gaps are related to constraints from the satellite design in terms of energy con-

[3] The ARF is a right-handed orthogonal frame with origin in the ARP, with the x_{ARF}-axis (commonly called East direction) pointing into the x_{SBF}-direction (nominal velocity direction), the y_{ARF}-axis (commonly called North direction) pointing into the $-y_{\mathrm{SBF}}$-direction and the z_{ARF}-axis (commonly called Up direction) pointing into the $-z_{\mathrm{SBF}}$-direction (zenith-pointing).

Table 2
GPS data availability for the three analyzed Spire satellites in the time frame 1 May-31 October 2020 (184 days). The number of days with RINEX files are given, as well as the average relative amount of available epochs per daily RINEX file. The latter is given taking into account all epochs, epochs for which at least 1 or 4 GPS satellites are tracked on both frequencies, and epochs with measurements on L1 only.

		Average available epochs [%]		
Satellite	Available days	Total	Dual freq. for at least 1/ 4 sat.	Only L1
FM099	161	74.5	74.0/ 73.9	0.6
FM103	184	69.3	68.8/ 68.7	0.6
FM115	100	69.1	68.7/ 68.7	0.4

sumption and conflicting hardware subsystems (Cappaert et al., 2021). Fig. 2 shows the evolution of the three daily duty cycles. It can be seen that FM115 has the highest duty cycles until mid of August, but then dropping significantly for the remaining days. The duty cycles for FM103 show a marked decrease between May and mid-July and an increase again until September, after which they remain more constant. The daily concatenated RINEX files contain in average 8.6, 8.1 and 7.0 data gaps with a median duration of 34.3 min, 34.8 min and 23.8 min for FM099, FM103 and FM115, respectively.

Fig. 3 shows the histogram of the epoch-wise number of tracked GPS satellites over the entire analyzed time span. It shows that for most epochs the number of tracked satellites is between 6 and 10. At the beginning of the analyzed time interval the maximum number of tracked satellites is 10 for all analyzed Spire LEOs. From July 3, August 19, and September 18 on, FM115, FM099 and FM103 started to track also up to 11 satellites (on August 31 FM099 even tracked 12 satellites for 87 epochs), likely due to an update of receiver settings.

Fig. 4 shows the distribution of available GPS observation for FM099 and one example day w.r.t. to the local zenith angle. It can be seen that more than 10 % of the observations are collected below the local horizon of the antenna. In this study, these observations are discarded due to an applied elevation cutoff of 0 ° (see Section 3).

Fig. 5 shows the signal-to-noise ratio C/N_0 as reported in the RINEX file for FM103 as a function of elevation. The S1C values (i.e., the signal-to-noise ratios for the observations on L1 C/A) range from 45–47 dB-Hz at zenith and decrease to 28–38 dB-Hz at zero elevation.

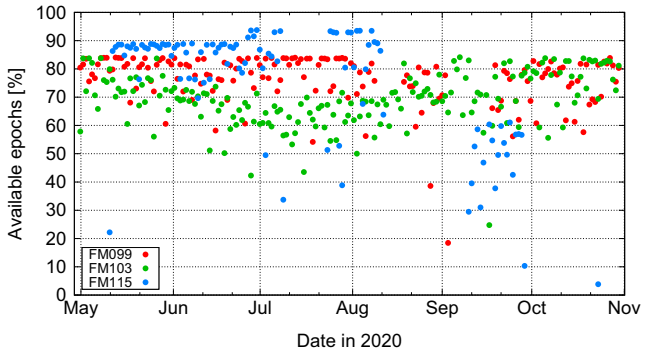

Fig. 2. Percentage of available epochs in daily RINEX files (duty cycles).

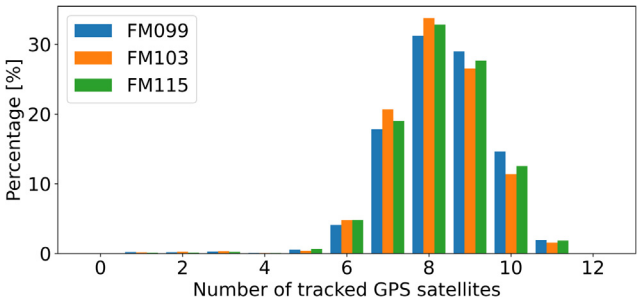

Fig. 3. Histogram of epoch-wise tracked number of GPS satellites for May-October 2020. The total number of epochs shown here amount to 10'630'247, 11'020'205, and 6'504'756 for FM099, FM103 and FM115, respectively.

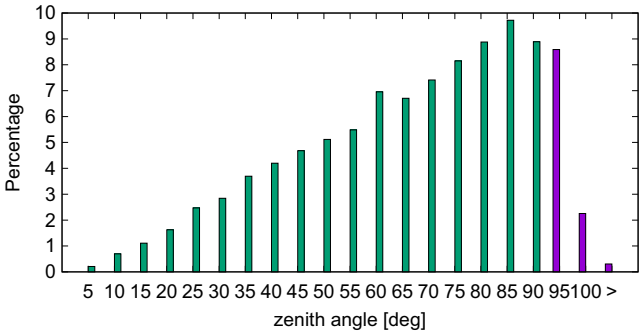

Fig. 4. Histogram of FM099 GPS observation distribution over different zenith angles for one example day.

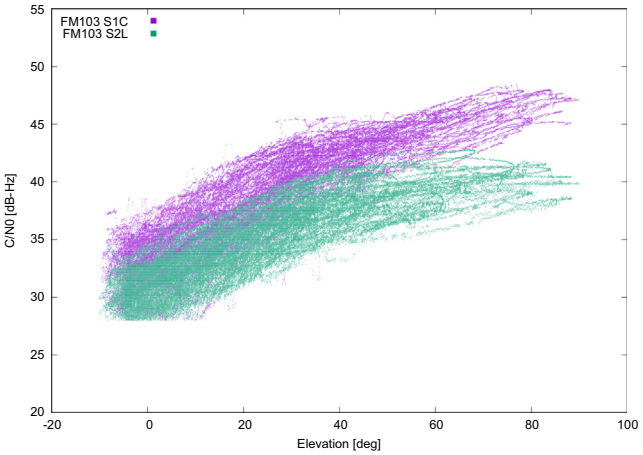

Fig. 5. C/N_0 (dB-Hz) values for FM103 for the time span 05:52–11:59 on May 13, 2020. A sharp cut is visible at 28 dB-Hz.

The signal-to-noise values S2L for the observations on L2 are slightly lower, ranging from 38–41 dB-Hz at zenith to 28–34 dB-Hz at zero elevation. These C/N_0 values are slightly lower than, e.g., for the scientific LEO satellite Sentinel-1A (Torres et al., 2012), which is equipped with an 8-channel GPS receiver provided by RUAG Space (Zangerl et al., 2014), and where the S1C C/N_0 values range between 50–60 dB-Hz at zenith. Fig. 5 again reveals that there are observations available which are significantly below the local horizon. Furthermore, it is visible that there is a sharp cut of C/N_0 values at 28 dB-Hz. Likely, the latter is due to the omission of GPS observations with lower signal-to-noise ratios before or at RINEX generation.

A peculiarity of the GPS data is found when analyzing the Melbourne-Wübbena linear combination of dual-frequency code and phase observations (Teunissen and Montenbruck, 2017). While this linear combination should show pass-wise constant values with noise dominated by code observations, in case of GPS data tracked by the Spire satellites many passes show large ramps of a few seconds up to several minutes length at the start or end of the pass. They indicate inconsistencies between the different observation types during these time periods, the reason is currently unknown to us. The affected data are screened away in the POD pre-processing.

Attitude quaternion data are provided by Spire in files spanning about 2 h data arcs (Level 1A leoAtt product, version 6.01). Each epoch in the leoAtt files carries a flag with the following meaning: 0: valid quaternion produced from the ADCS, 1: quaternion was missing and the last known quaternion was filled instead, 2: quaternion was missing and a default quaternion of (0,0,0,1) was filled instead. Like in the case of GPS data, different leoAtt files usually contain overlapping data epochs. But unlike for GPS data, the actual attitude information of one and the same epoch can be different in different leoAtt files. In particular, numerous epochs with a flag 0 or 1 are in later leoAtt files flag-2 epochs. In some cases flag-1 epochs keep a flag 1, but the quaternion values change in later leoAtt files, and in some cases flag-1 or flag-2 epochs become a flag-0 epoch later. When concatenating the leoAtt files for a daily processing, there are then different possibilities for handling overlapping epochs. In the BSW processing (see Section 3) always the quaternions with the lowest flags were used in the concatenation, while in the Napeos processing the quaternions from the latest data arc-wise leoAtt file were taken.

The attitude data are more complete than the GPS data, for most days there are quaternions available at each second. The average daily availabilities over the entire analyzed time span amount to 97.9 % for FM099 and FM103, and 92.8 % for FM115.

3. POD methods

For this study, precise orbits of the considered Spire nano satellites are computed using two different state-of-the-art processing software packages, Bernese GNSS Software (BSW, Dach et al., 2015) and ESA's Napeos software (Springer et al., 2011). Both software packages are employed to independently compute reduced-dynamic orbit solutions (Wu et al., 1991) using the ionosphere-free linear combination of undifferenced GPS observations in a 24 h batch least-squares processing using a Precise Point Positioning (PPP, Zumberge et al., 1997) approach, with GPS orbits and clock corrections fixed. Table 3 summarizes the employed GPS measurement models, as well as the orbit models and parametrizations for the reduced-dynamic POD. As can be seen, the Napeos processing includes an explicit modeling of non-conservative forces (due to solar radiation pressure and air drag), while in the BSW processing these forces are modeled in a purely empirical way by means of empirical and pseudo-stochastic orbit parameters. Such a difference in the handling of non-conservative forces can lead to useful insight related to satellite center of mass location or sensor offset errors (Peter et al., 2017; Mao et al., 2021). This is because the more reduced-dynamic orbit solutions obtained with BSW are more susceptible to such errors, while the leveling of the Napeos-derived orbits is driven to a larger extent by the physical models. The constant surface area of 0.12 m^2 used for atmospheric drag and solar radiation pressure in the case of Napeos processing is a very rough guess due to lack of information about the correct satellite geometry for this study.

In addition to reduced-dynamic orbit solutions, kinematic orbit solutions (Švehla and Rothacher, 2002), i.e., epoch-wise three-dimensional positions, are computed using the BSW. The latter are derived in a purely geometrical positioning, do not make use of any LEO satellite orbit dynamics and allow for an internal consistency check.

For both processings the operational final GNSS products (orbits, clocks, code and phase biases and Earth rotation parameters) of the Center for Orbit Determination in Europe (CODE) were used (Dach et al., 2020). Until day 20/137 (16 May 2020) they are given in the reference frame IGS14 (Rebischung, 2016), from day 20/138 on in IGb14 (Rebischung, 2020).

Next to the orbit parameters listed in Table 3, epoch-wise receiver clock corrections (for the reduced-dynamic and the kinematic orbits), as well as carrier phase ambiguity parameters were estimated. Tests were performed to fix the carrier phase ambiguities to their integer values using single-receiver ambiguity resolution strategies (Schaer et al., 2021). In case of the BSW processing the usually employed sigma-dependent ambiguity resolution strategy (Dach et al., 2015) was not successful to fix widelane ambiguities. This is explained by the rather noisy pseudorange GPS data (see Section 5.1), which leads to large formal errors of the ambiguity parameters, rendering the resolution strategy ineffective. As will be shown in Section 6.1, the problems with ambiguity resolution are not related to the significant gaps in the Spire data. Tests with an increase of the data sampling to 1 Hz (decreasing the noise) have

Table 3
Summary of models and parameters employed for reduced-dynamic Spire orbit determination.

	Bernese GNSS Software	Napeos
GPS Measurements		
GPS observations	ionosphere-free linear combination of undifferenced GPS L1/L2 carrier phase measurements (σ_L = 1 mm on L1/L2); 10 s sampling; 0 ° elevation cutoff	ionosphere-free linear combination of undifferenced GPS L1/L2 pseudorange (σ_P = 2.0 m on L1/L2) and carrier phase (σ_L = 10 mm on L1/L2) measurements; 10 s sampling; 0 ° elevation cutoff
GPS orbits, clocks and biases	CODE final product; 5 s clocks (Dach et al., 2020; Bock et al., 2009)	CODE final product; 5 s clocks
GPS satellite antennas	igs14.atx (Schmid et al., 2016; Rebischung, 2016)	igs14.atx
Spire GPS antennas	PCO from Spire, PCV from inflight calibration	PCO from Spire, PCV from inflight calibration
Spire attitude	measured quaternions	measured quaternions
Reference frame	IGS14/IGb14 (Rebischung, 2016; Rebischung, 2020)	IGS14/IGb14
Phase wind-up	modelled (Wu et al., 1993)	modelled
Orbit Model		
Earth gravity field	GOCO06s (Kvas et al., 2021)	EIGEN-GRGS-RL04 (Lemoine et al., 2019)
Ocean tides	EOT11a (Savcenko and Bosch, 2012)	FES2014 (Lyard et al., 2021)
Solid Earth and pole tides	IERS2010 (Petit and Luzum, 2010)	IERS2010
Solar radiation pressure	n.a.	constant area (0.12 m^2)
Earth radiation pressure	n.a	n.a.
Atmospheric forces	n.a.	NRLMSISE-00 (Picone et al., 2002), constant area (0.12 m^2)
Orbit parameters		
Initial conditions	arc-wise initial osculating elements	arc-wise initial state vector
Estimated scale factor	n.a.	SRP fixed to 1.0; 1 drag coefficient fixed to 1.0
Empirical acceleration	arc-wise constant accelerations in radial (R), tangential (T) and normal (N) direction, piecewise-constant RTN accelerations at 6 min intervals (σ = 10 nm/s^2)	12 sets of cycle-per-revolution (CPR) parameters in T and N (constant, sine + cosine (σ = 0.01 m/s^2))

shown that the fixing of ambiguities becomes possible to a certain extent, however significantly increasing processing time. Due to the encountered difficulties w.r.t. ambiguity fixing it was decided to only analyze ambiguity-float orbit solutions for this study. Consequently, in the BSW processing code data is only used for receiver clock synchronization with GPS time, while the final POD is based on carrier phase data only. The Napeos processing made use of both code and phase data with a fixed relative weight (see Table 3).

4. Antenna calibration

Prerequisite for GPS-based POD with an accuracy of few cm is a proper calibration of the receiver antenna phase center variations (PCVs, Jäggi et al., 2009). Spire provided ground-calibrated PCV patterns for the LEMUR 3.1.0 antenna for GPS L1 and L2 frequencies (Fig. 6). The convention used for these ground-calibrated PCVs (azimuth is counted counter-clockwise from x- to y-axis of the ARF; V. Nguyen, personal communication, November 2021) differs from the commonly used convention for LEO GNSS antennas (azimuth is counted clockwise from y- to x-axis of the ARF, Rothacher and Schmid, 2010; Jäggi et al., 2009). The different understanding of the conventions might be the cause for the different visualization of the L1 pattern in Allahvirdi-Zadeh et al. (2022) (see their Fig. 6 left).

Although ground-calibrated values are available, an in-flight calibration of the PCV pattern based on carrier phase residuals of the ionosphere-free linear combined observations is done in several iterations. Results from other LEO satellites have shown that ground-calibrated PCV patterns normally do not reflect the real flight environment and an in-flight calibration is necessary. The carrier-phase residuals of the ionosphere-free observations over a longer time series (approx. six months in this case) are binned according to the azimuth and elevation of the corresponding measurements. Commonly, $1^\circ \times 1^\circ$ bins are generated and the residuals are averaged. These values are then introduced as corrections into the next iteration and the procedure is repeated several times until the delta correction to the PCV pattern is marginal, normally after 3–5 iterations.

The in-flight calibration is done with both software packages and for the three processed Spire satellites independently. Fig. 7 shows the PCV patterns derived with Napeos and BSW. The differences between the ground-calibrated PCV pattern and the in-flight calibrations can be noticed and they confirm the necessity of the in-flight calibration. The variations between the patterns of FM099, FM103, and FM115 are not expected, because the satellites have the same satellite bus version. Other identically constructed satellites, as for instance the three ESA Swarm satellites (Friis-Christensen et al., 2008), have much more similar antenna PCVs (van den IJssel et al., 2015). Also PCV maps for other than the analyzed Spire

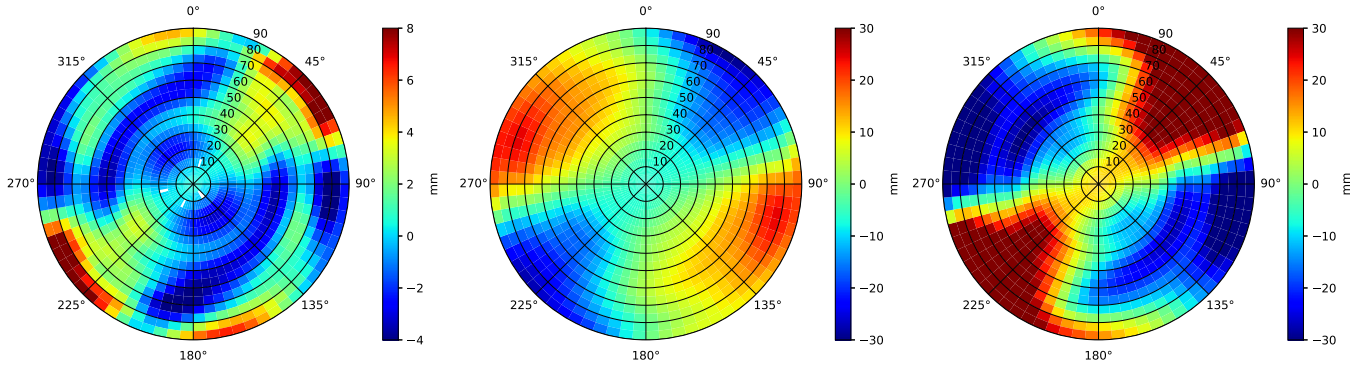

Fig. 6. Spire PCV patterns from ground calibration for L1 (left), L2 (center) and the ionosphere-free linear combination of L1 and L2 (right). The patterns are displayed in the commonly adopted convention of counting azimuth clockwise from y- to x-axis of the ARF.

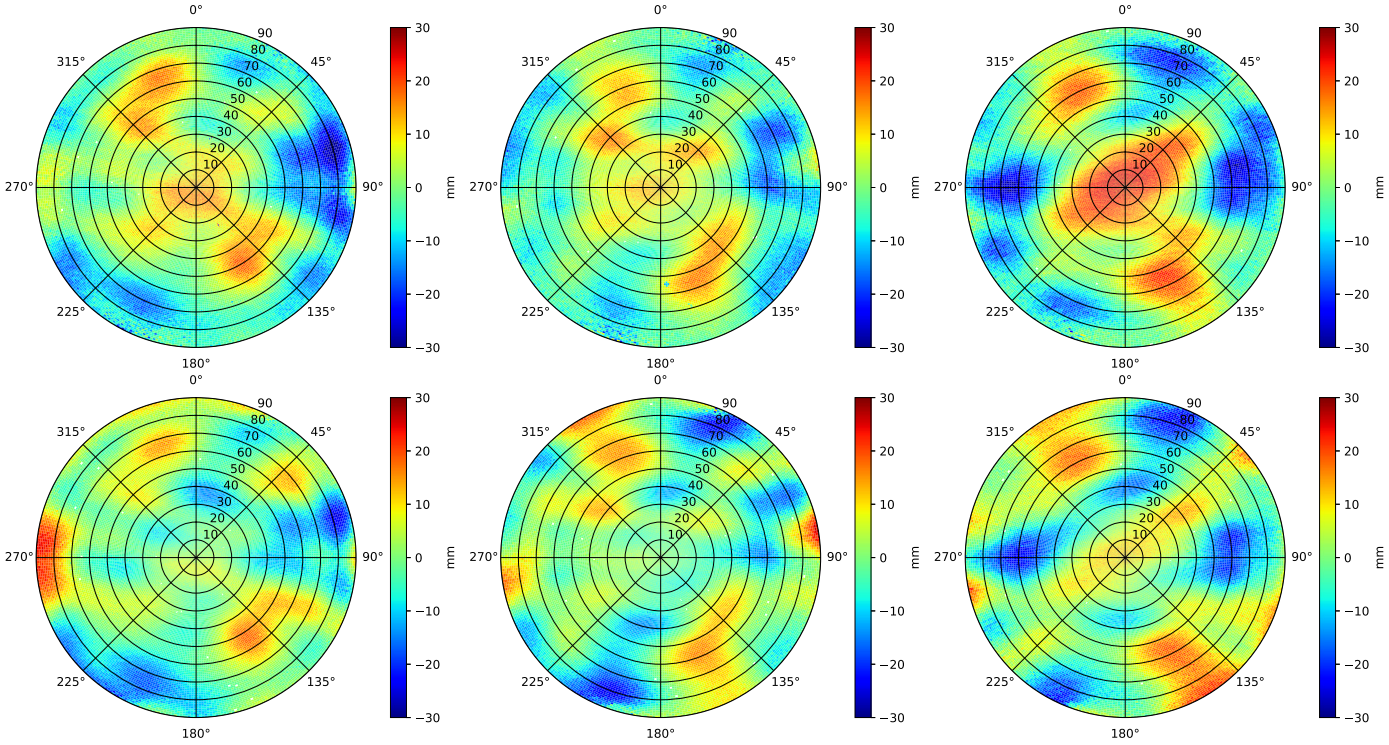

Fig. 7. Spire PCV patterns derived from ionosphere-free carrier phase residuals for FM099 (left), FM103 (center), and FM115 (right) from the Napeos (top) and BSW (bottom) processing.

satellites have been computed. While, e.g., the satellites FM099, FM101 and FM102 are all of identical bus version, in Sun-synchronous orbits with LTAN 09:30 and at identical altitude, also their patterns show very obvious differences. From this it can be concluded that the differences in the PCV patterns cannot be explained only by SRP-related modeling deficiencies impacting the in-flight calibrated patterns. Due to the differences between the PCV patterns of the three Spire satellites it is not recommended to use a common PCV pattern for all Spire satellites.

Differences between the PCV patterns from Napeos and BSW may have their cause in the orbit parametrization. Peter et al. (2017) showed that in the case of not perfectly known satellite geometry a more dynamically aligned parametrization with few empirical parameters as in the case of Napeos may lead to induced offsets in the PCV pattern.

5. Orbit results

In this section the quality of the individually determined orbit solutions is discussed, and the solutions are intercompared and compared to the official solutions provided by Spire. Furthermore, empirical and non-gravitational accelerations and receiver clock corrections are analyzed.

5.1. Code and carrier phase residuals

Fig. 8 shows, for the example day of 1 May 2020, pseudorange and carrier phase residuals obtained in the reduced-dynamic POD using Napeos. Residuals for Spire FM099 are shown. For comparison, the corresponding residuals for the POD of the scientific Earth observation satellite Sentinel-3B (Donlon et al., 2012) are displayed. For the Spire satellite the regular data gaps due to a duty cycle of less than 100 % can be observed. Furthermore, it is visible that especially the code residuals for FM099 are markedly larger than for Sentinel-3B. Fig. 9 shows the daily RMS values of pseudo-range and carrier phase residuals from the reduced-dynamic POD for all three analyzed Spire satellites and for the BSW and Napeos processing. Firstly, this figure confirms the relatively large code residuals for all days and satellites analyzed. Secondly, the general pseudo-range RMS values are markedly larger for the BSW processing than for the Napeos processing. This can be explained due to the fact that in the Napeos processing pseudo-range residuals were edited with a threshold of 10 m (see also Fig. 8), while in the BSW processing the editing threshold was set to 1000 m to only remove the largest outliers (recall that, apart for receiver clock synchronization with GPS time, the BSW processing did not make use of pseudo-range data for the POD).

The ionosphere-free carrier phase residuals are on a level of 8–9 mm and rather comparable for the BSW and Napeos processing. These values are a factor 2–3 larger than what is usually obtained when fitting GPS carrier phase data of scientific Earth observation satellite receivers. In average, the smallest carrier phase (and also pseudorange) residuals are obtained for FM115, which is the highest of the three analyzed satellites and thus the least affected by air drag and ionospheric perturbations (Jäggi et al., 2016). It has to be noted that in the case of the Napeos processing, in order to obtain good orbit results

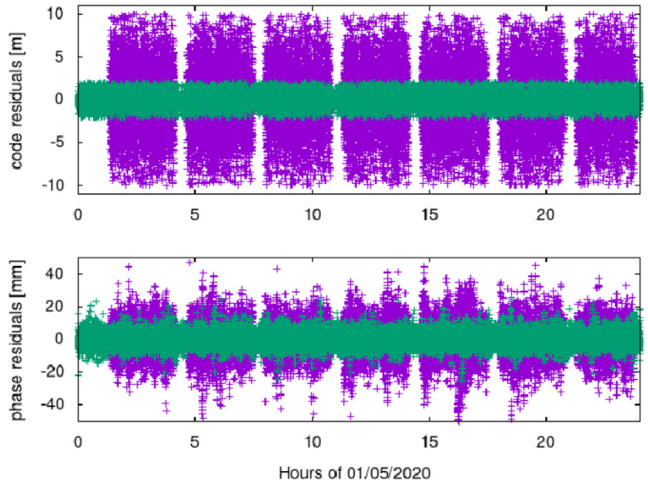

Fig. 8. Pseudorange (top) and carrier phase (bottom) residuals for Spire FM099 (purple) and Sentinel-3B (green) from Napeos processing for one example day.

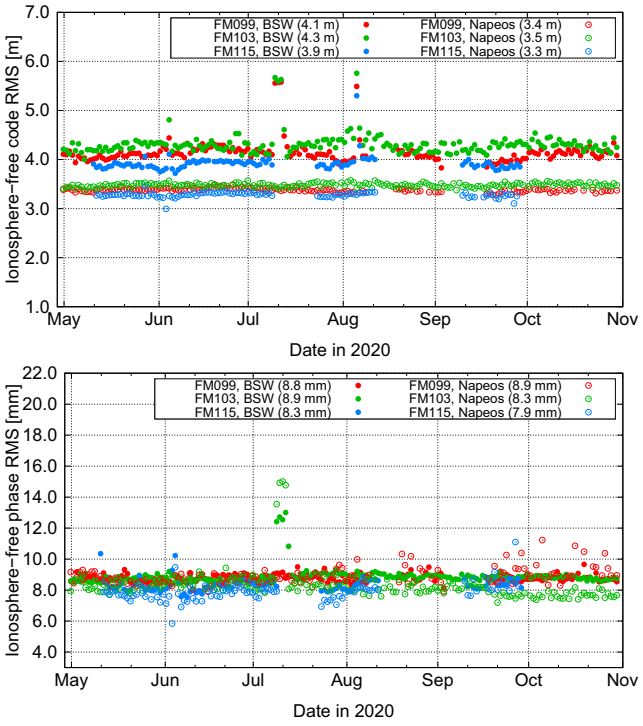

Fig. 9. Daily RMS values of ionosphere-free pseudorange (top) and carrier phase (bottom) residuals of reduced-dynamic POD for the three Spire satellites, and for the BSW (filled circles) and Napeos (empty circles) processing. The numbers in parentheses denote the average values.

with the chosen processing strategy and parametrization, the orbit arc length had to be adjusted for 30, 42 and 18 days for FM099, FM103 and FM115, with the shortest arc spanning only 8 h. The BSW processing, on the other hand, made use of 24 h orbit arcs for all days. Fig. 10 shows the daily carrier phase residuals from the kinematic POD in the BSW processing. Also these residuals are on a level of 8–9 mm, and in average again smallest for FM115. For FM103 a clear increase of carrier noise from day 191 (9 July 2020) onwards can be observed. Fig. 10 also shows the daily mean total electron content (TEC) values of the iono-

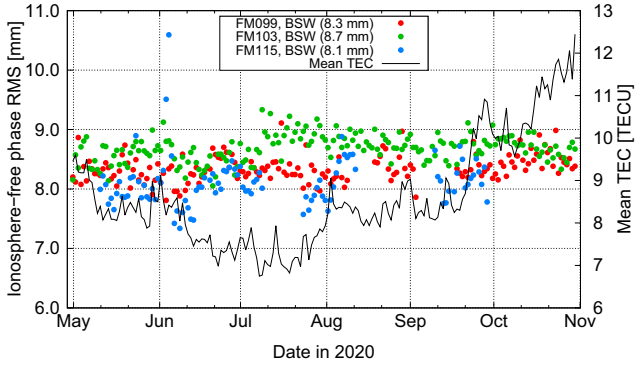

Fig. 10. Daily RMS values of ionosphere-free carrier phase residuals of kinematic POD for the three Spire satellites in the BSW processing, as well as daily mean TEC values. The numbers in parentheses denote the average values. 1 TECU = 10^{16} electrons/m^2.

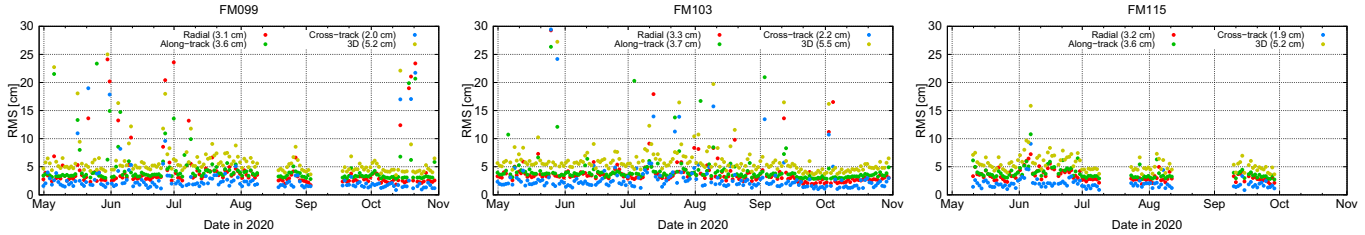

Fig. 11. Daily RMS differences between reduced-dynamic and kinematic orbits from the BSW processing in the local orbit frame. Orbit differences larger than 5 m have been excluded from the statistics. For FM099 and FM103, on 4 and 2 days RMS values above 30 cm occur and are not shown, respectively. The values in parentheses denote the median values.

sphere as determined by CODE. It can be seen that in 2020 the ionospheric activity was still rather low and the slight increase of mean TEC towards the end of the period does not seem to be reflected in the carrier phase noise.

5.2. Comparison of reduced-dynamic and kinematic orbits

The comparison of the reduced-dynamic and kinematic orbit solutions from the BSW processing provides an internal consistency measure. Kinematic orbits are fully independent of the Spire satellite dynamics, but are most sensitive to data quality. Fig. 11 shows the daily RMS differences between the BSW reduced-dynamic and kinematic orbits. The two orbit types agree on a level of 5.2–5.5 cm 3D RMS. For FM103 the improved GPS data tracking from mid September onwards (see Fig. 2) translates into a visibly better consistency between the two orbit types. The observed consistency is slightly worse than what is usually achieved for scientific Earth observation satellites (Mao et al., 2021; Arnold et al., 2023).

5.3. Comparison of Napeos and BSW-derived orbits

Fig. 12 shows the differences of the reduced-dynamic orbit solutions from the BSW and Napeos processing for FM103 and day 20/142 (21 May 2020). It shows that, typically, the two independent reduced-dynamic orbit solutions agree on a level of a few centimeters for positions and a few hundredths mm/s for velocities (in terms of median and median absolute deviation, MAD[4]). However, during times with no or only single-frequency GPS data in the RINEX files (gray areas in Fig. 12) significantly larger differences can show up. This can be explained by empirical parameters which are only weakly determined during these time intervals, causing the two differently parametrized orbits to diverge. Fig. 12 also reveals a radial offset of 3 cm between the two orbit solutions.

Fig. 13 shows the daily RMS differences for the three satellites and all analyzed days. Only orbit differences for time periods with dual-frequency GPS data have been used to compute the RMS values, and additional outliers

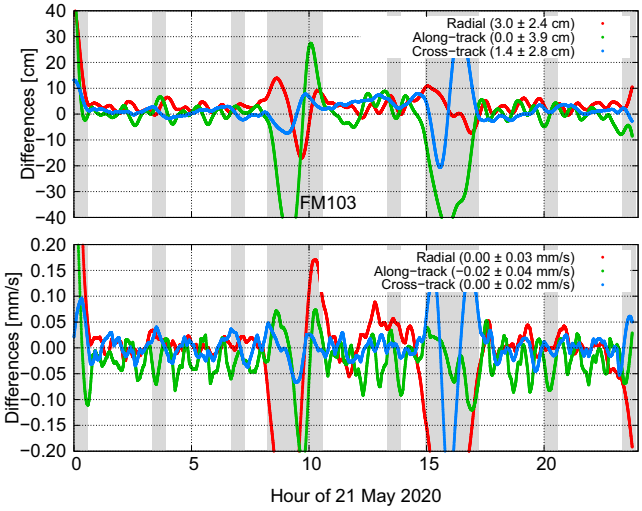

Fig. 12. Differences of reduced-dynamic orbits from BSW and Napeos processing for FM103 and day 20/142. The top plot shows position differences, the lower plot velocity differences, both in the local orbital frame. The gray areas mark times during which no or only single-frequency GPS data were available in the RINEX file. The numbers in parentheses denote the median and median absolute deviation (MAD) values.

exceeding 5 m for positions and 10 mm/s for velocities have been removed. In general, the two orbit solutions agree on a level of 6–7 cm 3D RMS in terms of positions and 0.05–0.06 mm/s in terms of velocities. The best agreement is visible for FM115, the highest of the three analyzed satellites. For FM099 a marked dispersion for the last two months can be seen. This is also reflected in the slightly larger daily RMS values of phase residuals for the Napeos processing, see Fig. 9. Table 4 summarizes the median values of daily mean and RMS differences, both for the case of using all daily orbit information, as well as only epochs with GPS data. In the latter case the two orbit solutions agree on a level of 2.3–4.8 cm or 0.02–0.05 mm/s in terms of 1D RMS. The agreement is markedly degraded, especially for FM099 and FM103, if orbits are compared for all epochs, including epochs during which no GPS data are available and where the orbit is thus obtained by pure inter- or extrapolation (see also Fig. 12). A mean radial offset of 2.5–3.5 cm between the two orbit solutions (mentioned earlier) is visible for all satellites. As will be shown in Section 5.5, this radial offset is in line with a correspond-

[4] For a data set $x_1,\ldots,x_n$ we define the (scaled) MAD as $\mathrm{MAD} = 1.4826 \cdot \mathrm{median}\left(|x_i - \mathrm{median}(x_j)|\right)$, which is a robust estimator for the standard deviation.

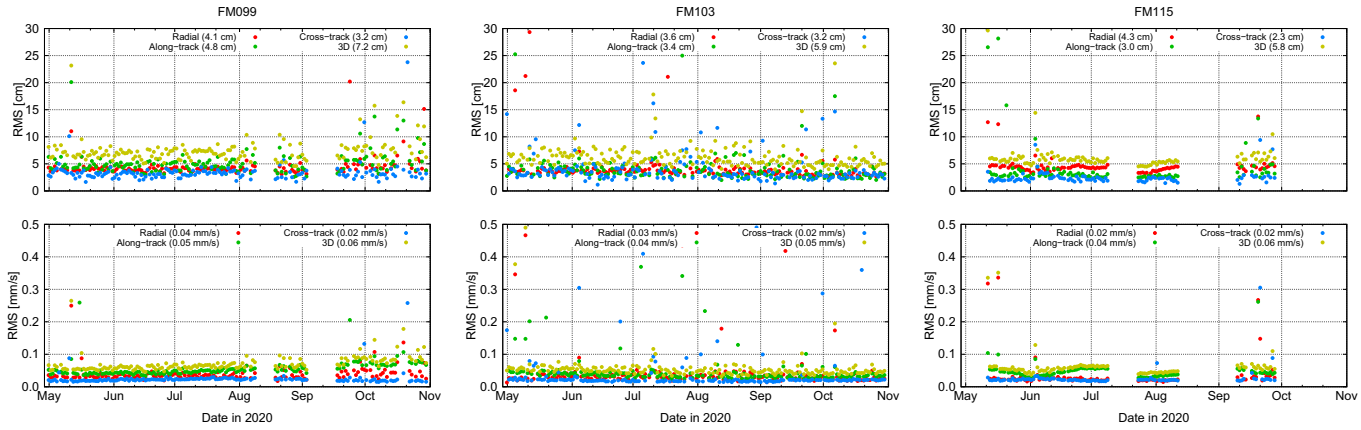

Fig. 13. Daily RMS differences between BSW- and Napeos-derived reduced-dynamic Spire orbits in terms of positions (top) and velocities (bottom) in the local orbital frame. For each day, only orbit information during epochs with dual-frequency GPS data available in the RINEX files were used. In addition outlier thresholds of 5 m for positions and 10 mm/s for velocities were applied. The numbers in parentheses denote the median RMS values.

ing difference in radial empirical accelerations between the two solutions.

5.4. Differences to Spire orbit solutions

The derived orbit solutions have been compared to the orbit products provided by Spire. Two different orbit solutions from Spire were delivered as part of the ESA AO data package: the Level 1A Rx Navigation Solution (podObs), containing the coarse estimates as computed by the onboard receiver, as well as the Level 1B Precise Orbit Determination Solution (leoOrb), derived by Spire's POD software RTOrb (Spire, 2021), which makes use of an extended Kalman filter. Both orbit solutions are in version 6.01 and contain the Spire satellite positions, velocities and receiver clock corrections in the IGS08 reference frame (Rebischung et al., 2012). The orbit products are delivered in a modified SP3-c format (Hilla, 2010), in which a three-digit integer instead of the letter 'L' and a two-digit integer is used to identify the satellite.

Table 4
Median values of daily orbit position (top) and velocity (bottom) differences in cm and mm/s between the BSW- and Napeos-derived reduced-dynamic orbits over the entire analyzed time span in the local orbital frame. Values for both the mean and RMS differences are shown. The values in columns "All epochs" were computed based on all epochs per day, the ones in "GPS data" only based on epochs with GPS data available. 5 m and 10 mm/s outlier thresholds were applied in the computation of daily mean and RMS values.

		All epochs		GPS data	
Satellite		Mean	RMS	Mean	RMS
FM099	R	2.8	5.0	2.9	4.1
	T	0.0	10.3	0.8	4.8
	N	0.2	3.6	0.0	3.2
FM103	R	2.5	10.8	2.7	3.6
	T	−0.2	25.7	0.0	3.4
	N	0.9	6.7	1.0	3.2
FM115	R	3.5	4.6	3.8	4.3
	T	0.1	4.5	0.1	3.0
	N	0.2	2.6	0.1	2.3

		All epochs		GPS data	
Satellite		Mean	RMS	Mean	RMS
FM099	R	0.00	0.10	0.01	0.04
	T	−0.03	0.06	−0.03	0.05
	N	0.00	0.03	0.00	0.02
FM103	R	0.00	0.29	0.00	0.03
	T	−0.02	0.11	−0.01	0.04
	N	0.00	0.05	0.00	0.02
FM115	R	0.00	0.04	0.00	0.02
	T	−0.04	0.06	−0.03	0.04
	N	0.00	0.02	0.00	0.02

Like in the case of RINEX data files, the Spire podObs and leoOrb products are provided in files spanning data arcs of lengths between less than 1 min and about 2 h. Consecutive files may have overlapping data epochs that can have different orbit information. For the comparison to the orbits computed in this study, these orbit files are concatenated to daily files, where always the orbit information of the latest file is retained.

Because the Spire orbit solutions computed with BSW and Napeos in this study are given in the IGS14 or IGb14 reference frames (as inherited by the reference frames of the employed GNSS products, see Section 3), there is a slight inconsistency of reference frames in the comparison to the IGS08-based Spire orbits. To transform ITRF2008 positions into ITRF2014, the following transformation is required[5]:

$$\vec{x}_{\mathrm{ITRF2014}} = \vec{x}_{\mathrm{ITRF2008}} + \vec{T} + D \cdot \vec{x}_{\mathrm{ITRF2008}}, \quad (1)$$

where $\vec{T} = (-1.6, -1.9, -2.4)$ mm and $D = 0.02 \cdot 10^{-9}$ are the translation and scale parameters, both valid at epoch 2010.0. The specified non-zero rates for the transformation parameters are 0.1 mm/y for the third translation component and $-0.03 \cdot 10^{-9}$/y for the scale. As a consequence,

[5] https://itrf.ign.fr/en/solutions/transformations.

for a satellite at 580 km altitude, the difference $|\vec{x}_{\mathrm{ITRF2014}} - \vec{x}_{\mathrm{ITRF2008}}|$ for mid 2020 varies between 0.8 and 4.9 mm, depending on the geographic location. In light of the significantly larger differences generally observed between the BSW- or Napeos-derived orbits and the Spire orbits, these frame inconsistencies are neglected in the following.

Fig. 14 shows the differences between the BSW reduced-dynamic orbit solution and the Spire leoOrb solution for FM103 and day 20/142 (21 May 2020), i.e., for the same satellite and day as in Fig. 12. These differences are about a factor 2.5–3.5 larger (by means of 1D MAD) than the differences between the BSW- and Napeos-derived reduced-dynamic orbits. Larger differences can be identified close to data gaps (gray areas), but sometimes also within time windows with GPS data. A peculiar feature is the presence of different smaller orbit arcs within a data batch, which are separated by smaller or larger jumps. Furthermore, it is obvious that the Spire leoOrb product only contains orbit information for epochs where GPS data are available.

Fig. 15 shows the daily RMS differences for the three satellites and all analyzed days. The general agreement of the BSW-derived and Spire leoOrb solutions amounts to 27–30 cm for positions and 0.32–0.36 mm/s for velocities in terms of 3D RMS. This position agreement matches roughly the typical accuracy estimates of the Spire POD solutions of 10–25 cm 3D RMS as specified in Spire (2021), but the velocity agreement is slightly worse than the 0.1–0.2 mm/s 3D RMS specified there. The best agreement is found for FM099, and for all satellites the differences are smallest in cross-track and largest in radial direction. The differences between the Napeos-derived orbits and the Spire leoOrb orbits are rather similar, apart from the radial offset: For FM103 and day 20/142 (cf. Fig. 14) the median of radial differences between Napeos-derived and Spire leoOrb orbits amounts to 0.5 cm. Notice that if the median radial differences w.r.t. Spire leoOrb are computed over the entire analyzed time span, they change to 1.6 cm and −0.9 cm for the BSW- and Napeos-derived orbits, respectively.

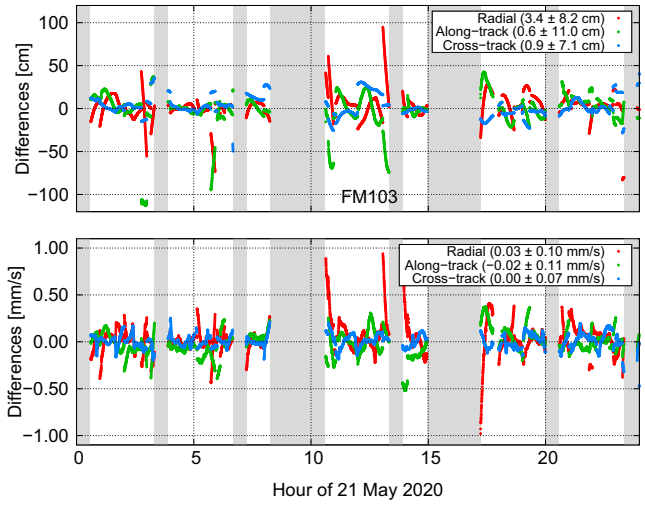

Fig. 14. Differences of reduced-dynamic orbits from BSW processing and Spire leoOrb solution for FM103 and day 20/142. The top plot shows position differences, the lower plot velocity differences, both in the local orbital frame. The gray areas mark times during which no or only single-frequency GPS data were available in the RINEX file. The numbers in parentheses denote the median and MAD values.

The along-track differences between the BSW-derived and the Spire leoOrb orbits in terms of velocities are at a level of 0.2 mm/s for all three analyzed satellites, which is at the upper bound of the range 0.05 – 0.2 mm/s, which is the generally required uncertainty for reliable radio occultation measurements (Teunissen and Montenbruck, 2017).

5.5. Empirical and non-gravitational accelerations

While the Napeos processing employed a simple explicit modeling of direct SRP and atmospheric drag accelerations, the BSW processing applied no physical models for these accelerations at all and addressed them only by means of empirically estimated accelerations (see Table 3). Fig. 16 shows these accelerations for FM103 and day 20/142 (the same satellite and day as shown in Figs. 12 and 14). For the BSW processing the sum of the constant and 6 minutes piecewise-constant accelerations are shown, for the Napeos processing the sum of explicitly modelled SRP and air drag, as well as the empirically estimated constant and CPR accelerations. In general, the BSW- and Napeos-derived accelerations show high correlations, but there is a clear offset of accelerations of about 100 nm/s^2 in radial direction. At the altitude of FM103 this directly corresponds to the above mentioned approximate 3 cm radial orbit offset between the two orbit solutions (Montenbruck et al., 2018), with the BSW-derived orbit lower than the Napeos-derived orbit. Due to the empirically estimated accelerations in radial direction, the BSW-derived orbit has almost no dynamical stiffness and is shifted in a one-to-one manner by erroneous offset vectors. Tests have shown that the radial offset between the BSW- and Napeos-based orbits becomes much smaller if, in the BSW processing, the empirical accelerations are replaced by an explicit non-gravitational force modelling comparable to the Napeos processing. This supports the assumption that the observed radial offset is indeed caused by an incorrect sensor offset vector from the satellite center of mass, rather than by some inconsistencies between the BSW and Napeos processing. Thus, the observed 3 cm radial orbit shift could be an indication that the assumed vector from satellite CoM to the GPS antenna reference point is too large by a comparable value in radial direction, i.e., that in the spacecraft body-fixed frame either the assumed CoM_z coordinate is too large or the POD ARP_z is too small, or a combination of these two cases. If the nominal PCV patterns provided by Spire (Fig. 6) contained a significant non-zero mean value in up direction, the corresponding PCO values might be inconsistent with the BSW-

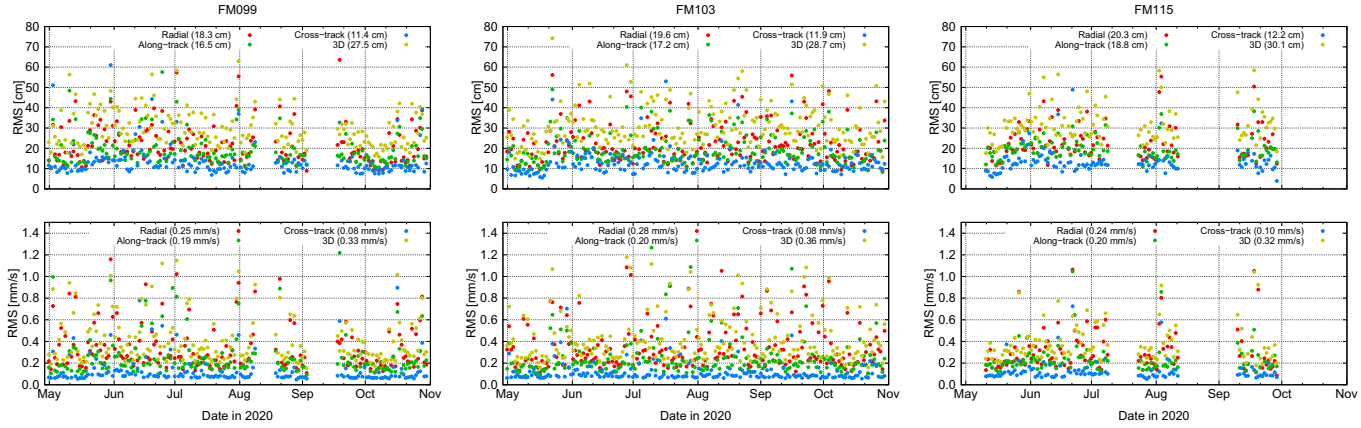

Fig. 15. Daily RMS differences between BSW reduced-dynamic and Spire leoOrb orbits in terms of positions (top) and velocities (bottom) in the local orbital frame. Outlier thresholds of 5 m for positions and 10 mm/s for velocities were applied. The numbers in parentheses denote the median RMS values.

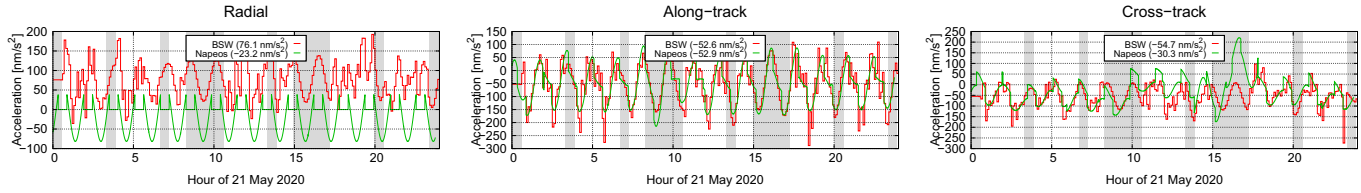

Fig. 16. Empirical and non-gravitational accelerations from the reduced-dynamic POD of FM103 on day 20/142 in the BSW and Napeos processing. The gray areas mark times during which no or only single-frequency GPS data were available in the RINEX file. The numbers in parentheses denote the mean values.

derived PCV pattern, which, due to orbit parametrization, does not contain any offset. However, POD tests with the nominal Spire PCV patterns in the BSW processing have revealed no significant radial orbit shift (a few mm in average), such that this error source can be ruled out.

5.6. Receiver clock corrections

The epoch-wise Spire receiver clock corrections, estimated as part of the parameters in the POD adjustment, turn out to exhibit relatively large drifts. This can be seen in Fig. 17, which shows the estimated corrections for the three analyzed satellites and one day. The drifts are compensated by regular jumps between the observation segments. The jumps are largest for FM103, amounting to several 10 ms. The stability of the individual segments can be assessed by means of the modified Allan deviation (MDEV), computed as in Eq. (3) of Allahvirdi-Zadeh et al. (2022). For the receiver clocks derived in the BSW processing and an averaging time $\tau = 60$ s, the means and standard deviations of MDEVs over all individual data segments in the analyzed time span amount to $(5.9 \pm 1.8) \cdot 10^{-9}$, $(1.1 \pm 0.6) \cdot 10^{-8}$ and $(5.7 \pm 2.0) \cdot 10^{-9}$ for FM099, FM103 and FM115, respectively. There is nearly no difference in stability between the receiver clocks obtained in the reduced-dynamic or kinematic POD. These numbers compare, e.g., to an MDEV($\tau = 60$ s) of $(1.8 \pm 0.6) \cdot 10^{-13}$ for the scientific Earth observation satellite GRACE-FO C in the same time period (values obtained by BSW using the same processing strategy as for Spire).

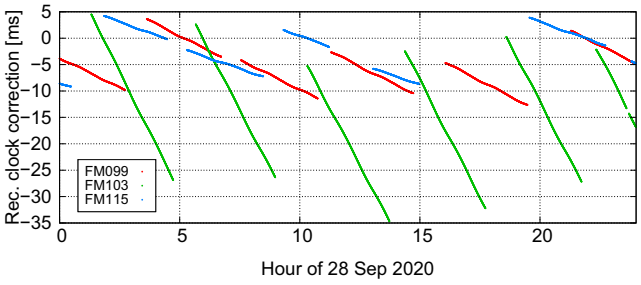

Fig. 17. Receiver clock corrections for day 20/272 (28 Sep 2020) from the BSW-based reduced-dynamic POD.

The large and drifting Spire clock corrections render the epochs of the kinematic positions in a kinematic POD to values which in general differ significantly from the integer seconds. This was similar for the GNSS receiver on ESA's Gravity field and steady-state Ocean Circulation Explorer (GOCE, Floberghagen et al., 2011), and must be taken into account if the kinematic orbits are to be used, e.g., for a subsequent Earth gravity field recovery.

6. Impact of data gaps on POD

As previously seen, the Spire data contain in average 7–9 data gaps per day with a typical duration of 25–35 min (see

Section 2.4). These gaps may pose difficulties to the reduced-dynamic POD, especially if use is made of empirical orbit parameters, which are not supported within the data gaps. In this section the question is addressed on how much the presence of data gaps affects the quality of the computed reduced-dynamic orbit.

6.1. Impact of data gaps on 24 h arcs

To illustrate the impact of gaps on an orbit which is determined in a 24 h arc, the following experiment was conducted. The orbit of the scientific LEO satellite GRACE-FO C was computed for day 20/142 in a 24 h arc using the BSW and employing the same strategy and parametrization as for Spire (cf. Table 3), in particular also with float carrier phase ambiguities. In this period the GRACE-FO satellites orbited the Earth at an altitude very similar to that of the Spire FM099 or FM103 satellites (about 500 km). The dynamical environment is thus comparable to the one present in the Spire POD. GRACE-FO C provided uninterrupted 10 s GPS data for the considered day, and the so-derived reduced-dynamic orbit can thus serve as an accurate reference. Then, artificial gaps were introduced to the GRACE-FO C GPS data, matching the data gaps for Spire FM103 on this day, and the GRACE-FO C POD was repeated (again using a 24 h arc). Fig. 18 shows the differences of the obtained orbit w.r.t. the reference orbit. As expected, the orbits differ most within the data gaps, with differences of more than 10 cm in along-track and more than 0.1 mm/s in radial direction. During epochs with GPS data the differences are smaller, but also reach up to 4.3 cm in along-track or 0.06 mm/s in radial direction. For this example these maximum values occur during the 6 minutes before midnight, where data are available again. From the point of view of RO applications these differences during periods with GPS data would be acceptable. However, the exact differences clearly depend on the employed orbit parametrization and might become larger in a more reduced-dynamic POD.

Finally, when attempting to fix carrier phase ambiguities to their integer values, it can be reported that the artificial introduction of gaps into the GRACE-FO data did not render the fixing impossible. For the considered day, compared to the case with continuous data, the number of set up ambiguities changed from 489 to 361 and the ambiguity fixing rate decreased from 86.5 % to 78.9 %. The gaps in the Spire data are thus not responsible for the observed problems w.r.t. ambiguity resolution in the Spire POD (see Section 3).

6.2. Comparison of daily and short arcs

An approach to handle the gaps in the Spire data can be to estimate one independent orbit arc (i.e., one set of initial conditions) for each continuous data segment. Compared to the estimation of one 24 h arc this approach increases the number of estimated orbit parameters. To analyze the impact of this strategy on the orbit solutions, GRACE-FO C orbits have been computed for day 20/142 using short arcs as defined by the corresponding Spire FM103 data segments. For each data segment the entire POD processing (including data screening) was repeated. Notice that for the short 6 minutes data segment before midnight no orbit was computed. Fig. 19 shows the difference of these short-arc orbits w.r.t. the reference orbit (obtained from complete data in a 24 h arc). It can be seen that for this example the differences are below 3 cm or 0.04 mm/s in 1D, and that they are generally larger at the beginning or the end of the short arcs. Again, these differences might be acceptable in view of pure RO applications, but also depend on the empirical orbit parametrization. While for the chosen parametrization the two choices of arc definition yield comparable results, the longer orbit arcs (e.g., 24 h) clearly allow for an easier incorporation of very short continuous data batches.

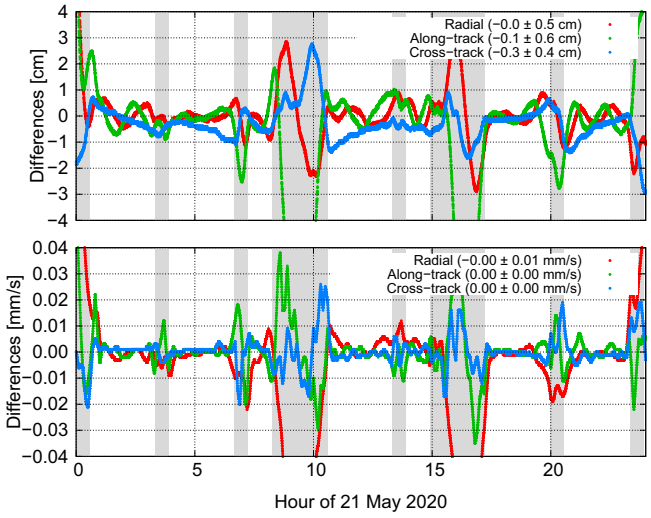

Fig. 18. Differences of the 24 h reduced-dynamic GRACE-FO C orbit obtained with gaps in the GPS data as for Spire FM103, compared to reference orbit obtained with complete data. The gray areas mark the data gaps. The numbers in parentheses denote the median and median absolute deviation (MAD) values.

7. Summary and conclusion

This paper addresses GPS-based POD of CubeSats from the Spire constellation. It summarizes technical details relevant for POD and presents results of the analysis of GPS tracking and attitude data of three representative Spire LEMUR2 satellites of major bus version 3.4 – FM099, FM103 and FM115 – for the time span May-October 2020 to characterize the general data quality and tracking performance. During the analyzed time span the Spire GPS data show numerous gaps of typically 25–35 minutes duration, amounting to average duty cycles of about 70–75 %. On most available epochs the number of tracked GPS satellites is between 6 and 11, which is very good and desirable for POD purposes.

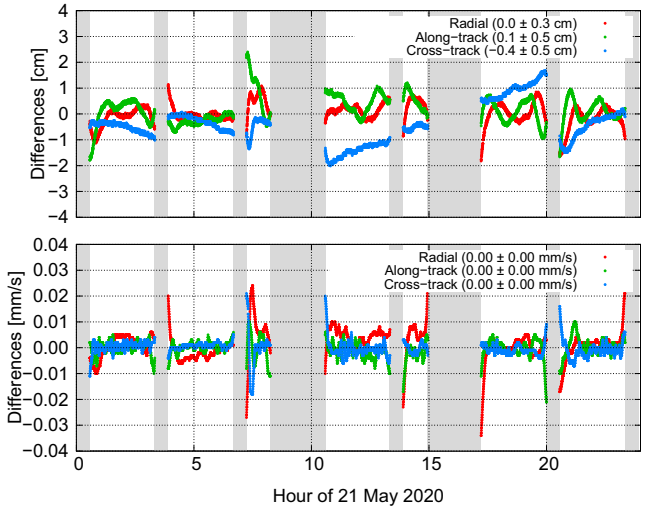

Fig. 19. Differences of the short-arc reduced-dynamic GRACE-FO C orbits obtained from the continuous GPS data segments defined by Spire FM103, compared to reference orbit obtained with complete data. The gray areas mark the data gaps. The numbers in parentheses denote the median and median absolute deviation (MAD) values.

The data were used for reduced-dynamic GPS-based POD by means of two independent state-of-the-art GNSS processing software packages, BSW and Napeos. The receiver antenna phase center variations were independently calibrated in flight and were found 1) to differ significantly from the ground-calibrated corrections provided by Spire, as well as 2) to show significant differences among the different (identically built) satellites. Due to the latter point it must be concluded that each individual Spire satellite requires an independent antenna PCV calibration and that it is not recommended to use a common PCV pattern for all Spire satellites.

A relatively large noise level of GPS code observations was found, impeding the fixing of widelane (and thus also narrowlane) carrier phase ambiguities to their integer values. As a consequence, only ambiguity-float solutions were analyzed in this work. Ionosphere-free phase residuals were found in the range of 8–9 mm RMS, which is moderately higher than what is obtained when using GPS carrier phase data of scientific Earth observation satellite receivers for POD.

The BSW was also used to derive independent kinematic orbit solutions, allowing to assess the internal orbit consistency. Generally, a similar carrier phase residual level as in the case of reduced-dynamic POD and a consistency of around 5 cm in 3D RMS between the two BSW-derived orbit types was found.

The BSW- and Napeos-derived reduced-dynamic orbits were intercompared and found to agree at the level of 6–7 cm or 0.05–0.06 mm/s in the sense of median 3D RMS. This is, however, only the case if the orbit comparison is restricted to epochs with dual-frequency GPS observations available. In particular for FM099 and FM103 a markedly worse agreement is found when including all orbit data, which is due to (different) empirical orbit parameters, which are weakly or not determined during data gaps. A systematic radial difference of about 3 cm between the BSW- and Napeos-derived orbits was found, which is consistent to the observed differences in empirical and non-gravitational accelerations between the two orbit solutions. The radial offset between the orbit solutions arises due to the different strategies to model non-gravitational accelerations acting on the Spire satellites. While Napeos made use of explicit physical models for direct solar radiation pressure and air drag, BSW absorbed these accelerations by means of empirical and pseudo-stochastic orbit parameters only. Tests have shown that the offset between the two solutions becomes significantly smaller if a comparable explicit modeling of non-gravitational forces is employed in the BSW processing as well. The observed offset might then be at least partially explained by erroneous antenna offset information which unequally affects the differently parametrized orbit solutions.

The reduced-dynamic satellite orbits derived by BSW were compared also to the official Level 1B POD solution provided by Spire (leoOrb product). In this case larger differences at the level of 27–30 cm or 0.32–0.36 mm/s 3D RMS were found. These comparisons hold for epochs with dual-frequency GPS data available, since the leoOrb ephemerides are given only during these epochs. In the along-track direction the BSW and Level 1B orbit velocities agree on a level of 0.2 mm/s, which is at the upper bound of accuracy required for radio occultation measurements.

Epoch-wise receiver clock corrections for both reduced-dynamic and kinematic orbit solutions were found to show relatively large drifts and regular jumps in the several 10 ms range. The clock stability was found to be similar to what was assessed by Allahvirdi-Zadeh et al. (2022).

Finally, the impact of the Spire data gaps on the orbit quality was assessed by artificially introducing corresponding gaps into the (continuous) GPS tracking data for GRACE-FO C. Both a 24 h arc and a short-arc (matching the Spire data batches) POD was performed to find that, during epochs with GPS data, the differences to the "true" orbit (obtained with continuous data) are in the range of a few cm or a few hundredths mm/s.

In summary, we have found that the GPS and attitude data quality collected by the analyzed Spire CubeSats is of very promising quality, allowing in general for a decent POD. As further steps the problem of the potentially erroneous GPS antenna offset (leading to the observed 3 cm radial orbit offset between BSW- and Napeos-derived solutions) needs to be further addressed and understood. In that context further orbit solutions shall be computed including detailed modelings of non-gravitational accelerations using satellite macro models. Furthermore, possibilities need to be explored to overcome the problems which the relatively large pseudorange noise pose to the widelane carrier phase ambiguity fixing. As is known from various scientific Earth observation LEO satellites, the proper fix-

ing of ambiguities leads to significantly more stable GNSS-derived orbit solutions and is thus also desirable for Spire POD.

Based on the presented experiences, a natural further step is then to use the POD-related data of the analyzed and of further Spire CubeSats for scientific applications like global geodetic parameter determination, Earth gravity field determination or ionospheric reconstructions.

Declaration of competing interest

The authors declare that they have no known competing financial interests or personal relationships that could have appeared to influence the work reported in this paper.

Acknowledgements

We acknowledge the support from Spire Global and the provision of Spire data by ESA in the frame of an Announcement of Opportunity (project No. 66978). This research was partly funded by the European Research Council under the grant agreement No. 817919 (project SPACE TIE). Calculations were partly performed on UBELIX (http://www.id.unibe.ch/hpc), the HPC cluster at the University of Bern.

References

Akyildiz, I.F., Kak, A., 2019. The internet of space things/CubeSats. IEEE Network 33 (5), 212–218. https://doi.org/10.1109/MNET.2019.1800445.

Allahvirdi-Zadeh, A., Awange, J., El-Mowafy, A., et al., 2022. Stability of cubesat clocks and their impacts on GNSS radio occultation. Remote Sens. 14, 362. https://doi.org/10.3390/rs14020362.

Angling, M.J., Nogués-Correig, O., Nguyen, V., et al., 2021. Sensing the ionosphere with the Spire radio occultation constellation. J. Space Weather Space Climate 11, 56. https://doi.org/10.1051/swsc/2021040.

Arnold, D., Grombein, T., Schreiter, L., et al., 2023. Reprocessed precise science orbits and gravity field recovery for the entire GOCE mission. J. Geodesy 97 (7), 67. https://doi.org/10.1007/s00190-023-01752-y.

Azami, M.H.b., Orger, N.C., Schulz, V.H., et al., 2022. Earth observation mission of a 6U CubeSat with a 5-meter resolution for wildfire image classification using convolution neural network approach. Remote Sens. 14 (8), 1874. https://doi.org/10.3390/rs14081874.

Bock, H., Dach, R., Jäggi, A., et al., 2009. High-rate GPS clock corrections from CODE: support of 1 Hz applications. J. Geodesy 83, 1083–1094. https://doi.org/10.1007/s00190-009-0326-1.

Cappaert, J., 2020. The Spire small satellite network. Handbook of Small Satellites: Technology, Design, Manufacture, Applications, Economics and Regulation, pp. 1–21. https://doi.org/10.1007/978-3-030-20707-6_93-1.

Cappaert, J., Foston, F., Heras, P.S., et al., 2021. Constellation modelling, performance prediction and operations management for the Spire constellation. In: Proceedings of the AIAA/USU Conference on Small Satellites, SSC21-I-13.

Dach, R., Lutz, S., Walser, P. et al., (Eds.) (2015). Bernese GNSS Software Version 5.2, Documentation. University of Bern, Switzerland. https://doi.org/10.7892/boris.72297.

Dach, R., Schaer, S., Arnold, D. et al., 2020. CODE final product series for the IGS. Published by Astronomical Institute, University of Bern; ftp://ftp.aiub.unibe.ch/CODE; https://doi.org/10.7892/boris.75876.4.

Donlon, C., Berruti, B., Buongiorno, A., et al., 2012. The global monitoring for environment and security (GMES) Sentinel-3 mission. Remote Sens. Environ. 120, 37–57. https://doi.org/10.1016/j.rse.2011.07.024.

da Encarnação, J.T., Visser, P., Arnold, D., et al., 2020. Description of the multi-approach gravity field models from Swarm GPS data. Earth Syst. Sci. Data 2, 1385–1417. https://doi.org/10.5194/essd-12-1385-2020.

Floberghagen, R., Fehringer, M., Lamarre, D., et al., 2011. Mission design, operation and exploitation of the Gravity Field and Steady-State Ocean Circulation Explorer mission. J. Geodesy 85 (11), 749–758. https://doi.org/10.1007/s00190-011-0498-3.

Forsythe, V.V., Duly, T., Hampton, D., et al., 2020. Validation of ionospheric electron density measurements derived from Spire CubeSat constellation. Radio Sci. 55 (1). https://doi.org/10.1029/2019RS006953, art. E2019RS006953.

Friis-Christensen, E., Lühr, H., Knudsen, D., et al., 2008. Swarm – an earth observation mission investigating geospace. Adv. Space Res. 41 (1), 210–216. https://doi.org/10.1016/j.asr.2006.10.008.

Grombein, T., Lasser, M., Arnold, D., et al., 2022. Determination and combination of monthly gravity field time series from kinematic orbits of GRACE, GRACE-FO and Swarm. In: Freymueller, J.T., Sánchez, L. (Eds.), Geodesy for a Sustainable Earth. Springer International Publishing, Cham, pp. 191–201. https://doi.org/10.1007/1345_2022_163.

Gunter, B.C., da Encarnação, J.T., Ditmar, P., et al., 2011. Using satellite constellations for improved determination of earth's time-variable gravity. J. Spacecraft Rock. 48 (2), 368–377. https://doi.org/10.2514/1.50926.

Haines, B.J., Bar-Sever, Y.E., Bertiger, W.I., et al., 2015. Realizing a terrestrial reference frame using the global positioning system. J. Geophys. Res.: Solid Earth 120 (8), 5911–5939. https://doi.org/10.1002/2015JB012225.

Hilla, S., 2010. The extended standard product 3 orbit format (SP3-c, National Geodetic Survey, National Ocean Service, NOAA).

Hoots, F., Roehrich, R., 1980. Models for propagation of NORAD element sets. Spacetrack report no. 3. https://doi.org/10.21236/ADA093554.

Huang, W., 2022. Enhancing GNSS by integrating low Earth orbiters, PhD Thesis. Technische Universität Berlin (Germany). https://doi.org/10.14279/depositonce-15101.

Hugentobler, U., Jäggi, A., Schaer, S. et al., 2005. Combined processing of GPS data from ground station and LEO receivers in a global solution. In: A Window on the Future of Geodesy: Proceedings of the International Association of Geodesy IAG General Assembly Sapporo, Japan June 30–July 11, 2003, Springer, pp. 169–174. https://doi.org/10.1007/3-540-27432-4_30.

van den IJssel, J., da Encarnação, J.T., Doornbos, E., et al., 2015. Precise science orbits for the Swarm satellite constellation. Adv. Space Res. 56 (6), 1042–1055. https://doi.org/10.1016/j.asr.2015.06.002.

Jäggi, A., Dach, R., Montenbruck, O., et al., 2009. Phase center modeling for LEO GPS receiver antennas and its impact on precise orbit determination. J. Geodesy 83 (12), 1145–1162. https://doi.org/10.1007/s00190-009-0333-2.

Jäggi, A., Dahle, C., Arnold, D., et al., 2016. Swarm kinematic orbits and gravity fields from 18 months of GPS data. Adv. Space Res. 57 (1), 218–233. https://doi.org/10.1016/j.asr.2015.10.035.

Johnstone, A., 2022. CubeSat Design Specification (1U–12U), Rev. 14.1. CP-CDS-R14.1 Cal Poly. URL: https://www.cubesat.org/s/CDS-REV14_1-2022-02-09.pdf.

Kłopotek, G., Schartner, M., Rothacher, M., et al., 2021. Exploring LEO cube satellite technology for space geodesy: SLR-VLBI POD in the GGOS era. In: EGU General Assembly Conference Abstracts EGU General Assembly Conference Abstracts, p. EGU21-1797. https://doi.org/10.5194/egusphere-egu21-1797.

Kopacz, J.R., Herschitz, R., Roney, J., 2020. Small satellites an overview and assessment. Acta Astronaut. 170, 93–105. https://doi.org/10.1016/j.actaastro.2020.01.034.

Kuang, D., Bar-Sever, Y., Haines, B., 2015. Analysis of orbital configurations for geocenter determination with GPS and low-earth orbiters. J. Geodesy 89, 471–481. https://doi.org/10.1007/s00190-015-0792-6.

Kulu, E., 2022. Nanosatellite launch forecasts-track record and latest prediction. In: Proceedings of the AIAA/USU Conference on Small Satellites, SSC22-S1-04..

Kvas, A., Brockmann, J.M., Krauss, S., et al., 2021. GOCO06s – a satellite-only global gravity field model. Earth Syst. Sci. Data 13 (1), 99–118. https://doi.org/10.5194/essd-13-99-2021, URL: https://essd.copernicus.org/articles/13/99/2021/.

Landerer, F.W., Flechtner, F.M., Save, H., et al., 2020. Extending the global mass change data record: GRACE Follow-On instrument and science data performance. Geophys. Res. Lett. 47 (12). https://doi.org/10.1029/2020GL088306, art. E2020GL088306.

Lemoine, J.-M., Biancale, R., Reinquin, F., 2019. CNES/GRGS RL04 earth gravity field models, from GRACE and SLR data. https://doi.org/10.5880/ICGEM.2019.010.

Lyard, F., Allain, D., Cancet, M., et al., 2021. FES2014 global ocean tide atlas: design and performance. Ocean Sci. 17, 615–649. https://doi.org/10.5194/os-17-615-2021.

Männel, B., Rothacher, M., 2017. Geocenter variations derived from a combined processing of LEO- and ground-based GPS observations. J. Geodesy 91, 933–944. https://doi.org/10.1007/s00190-017-0997-y.

Mao, X., Arnold, D., Girardin, V., et al., 2021. Dynamic GPS-based LEO orbit determination with 1 cm precision using the Bernese GNSS Software. Adv. Space Res. 67 (2), 788–805. https://doi.org/10.1016/j.asr.2020.10.012.

Montenbruck, O., Hackel, S., Jäggi, A., 2018. Precise orbit determination of the Sentinel-3A altimetry satellite using ambiguity-fixed GPS carrier phase observations. J. Geodesy 92 (7), 711–726. https://doi.org/10.1007/s00190-017-1090-2.

Palfreyman, A., Curial, A.d.S., Rawlinson, J. et al., 2022. Scouting for climate variable with small satellites. In: Proceedings of the AIAA/USU Conference on Small Satellites, Weekday Session V, SSC22-V-05.

Pastena, M., Tossaint, M., Regan, A., et al., 2020. Overview of ESA's earth observation upcoming small satellites missions. In: Proceedings of the AIAA/USU Conference on Small Satellites, Technical Session V, SSC20-V-04.

Peter, H., Jäggi, A., Fernández, J., et al., 2017. Sentinel-1A – First precise orbit determination results. Adv. Space Res. 60 (5), 879–892. https://doi.org/10.1016/j.asr.2017.05.034.

Petit, G., Luzum, B., 2010. IERS Conventions (2010). IERS Technical Note No. 36 Verlag des Bundesamts für Kartographie und Geodäsie Frankfurt.

Picone, J., Hedin, A., Drob, D., 2002. NRLMSISE-00 empirical model of the atmosphere: Statistical comparisons and scientific issues. J. Geophys. Res.: Space Phys. 107 (A12), 1468. https://doi.org/10.1029/2002JA009430.

Rebischung, P., 2016. Upcoming switch to IGS14/igs14.atx, IGSMAIL-7399, 21 Dec. 2016. URL: https://lists.igs.org/pipermail/igsmail/2016/001233.html.

Rebischung, P., 2020. Switch to IGb14 reference frame, IGSMAIL-7921, 14 Apr. 2020. URL: https://lists.igs.org/pipermail/igsmail/2020/007917.html.

Rebischung, P., Griffiths, J., Ray, J., et al., 2012. IGS08: the IGS realization of ITRF2008. GPS Solut. 16 (4), 483–494. https://doi.org/10.1007/s10291-011-0248-2.

Romero, I., 2020. The Receiver Independent Exchange Format Version 3.05. URL: https://files.igs.org/pub/data/format/rinex305.pdf.

Rothacher, M., Schmid, R., 2010. ANTEX: The Antenna Exchange Format, Version 1.4. URL: https://files.igs.org/pub/data/format/antex14.txt.

Saeed, N., Elzanaty, A., Almorad, H., et al., 2020. CubeSat communications: Recent advances and future challenges. IEEE Commun. Surv. Tutor. 22 (3), 1839–1862. https://doi.org/10.1109/COMST.2020.2990499.

Savcenko, R., Bosch, W., 2012. EOT11a – Empirical ocean tide model from multi-mission satellite altimetry. DGFI-Report No 89. Deutsches Geodätisches Forschungsinstitut, Munich. https://doi.org/10.10013/epic.43894.d001.

Schaer, S., Villiger, A., Arnold, D., et al., 2021. The CODE ambiguity-fixed clock and phase bias analysis products: generation, properties, and performance. J. Geodesy 95, 1–25. https://doi.org/10.1007/s00190-021-01521-9.

Schmid, R., Dach, R., Collilieux, X., et al., 2016. Absolute IGS antenna phase center model igs08.atx: status and potential improvements. J. Geodesy 90, 343–364. https://doi.org/10.1007/s00190-015-0876-3.

Schreiner, W.S., Weiss, J., Anthes, R.A., et al., 2020. COSMIC-2 radio occultation constellation: First results. Geophys. Res. Lett. 47 (4). https://doi.org/10.1029/2019GL086841, art. E2019GL086841.

Schreiter, L., Stolle, C., Rauberg, J., et al., 2023. Topside ionosphere sounding from the CHAMP, GRACE, and GRACE-FO missions. Radio Sci. 58 (3). https://doi.org/10.1029/2022RS007552, art. E2022RS007552.

Spire, 2021. Spire attitude and navigation product summary, rev. 1.0. URL: https://spire-earth-obs-product-documentation.s3.us-west-2.amazonaws.com/att-nav/spire_data_manual_att-nav_summary.pdf.

Springer, T., Dilssner, F., Escobar, D., 2011. NAPEOS: The ESA/ESOC Tool for Space Geodesy. Geophys. Res. Abstracts 13, EGU2011-8287.

Sutton, E.K., Thayer, J.P., Pilinski, M.D., et al., 2021. Toward accurate physics-based specifications of neutral density using GNSS-enabled small satellites. Space Weather 19 (6). https://doi.org/10.1029/2021SW002736, art. E2021SW002736.

Švehla, D., Rothacher, M., 2002. Kinematic orbit determination of LEOs based on zero or double-difference algorithms using simulated and real SST GPS data. In: Vistas for Geodesy in the New Millennium. Springer, pp. 322–328. https://doi.org/10.1007/978-3-662-04709-5_53.

Tapley, B.D., Bettadpur, S., Ries, J.C., et al., 2004. GRACE measurements of mass variability in the Earth system. Science 305, 503–506. https://doi.org/10.1126/science.1099192.

Teunissen, P., Montenbruck, O. (Eds.) 2017. Springer Handbook of Global Navigation Satellite Systems. Springer. https://doi.org/10.1007/978-3-319-42928-1.

Torres, R., Snoeij, P., Geudtner, D., et al., 2012. GMES Sentinel-1 mission. Remote Sens. Environ. 120, 9–24. https://doi.org/10.1016/j.rse.2011.05.028.

Wu, J.T., Wu, C., Hajj, G.A., et al., 1993. Effects of antenna orientation on GPS carrier phase. Manuscripta Geodaetica 18, 91–98.

Wu, S., Chen, W., Cao, C., et al., 2021. A multiple-CubeSat constellation for integrated earth observation and marine/air traffic monitoring. Adv. Space Res. 67 (11), 3712–3724. https://doi.org/10.1016/j.asr.2020.04.025.

Wu, S.-C., Yunck, T.P., Thornton, C.L., 1991. Reduced-dynamic technique for precise orbit determination of low earth satellites. J. Guidance Control Dyn. 14 (1), 24–30. https://doi.org/10.2514/3.20600.

Zangerl, F., Griesauer, F., Sust, M. et al., 2014. SWARM GPS precise orbit determination receiver initial in-orbit performance evaluation. In: Proc. ION GNSS+ 2014, pp. 1459–1468.

Zumberge, J.F., Heflin, M.B., Jefferson, D.C., et al., 1997. Precise point positioning for the efficient and robust analysis of GPS data from large networks. J. Geophys. Res.: Solid Earth 102 (B3), 5005–5017. https://doi.org/10.1029/96JB03860.